High-ZT from optimized carrier concentration and electron – phonon interaction in Cr-doped BiCuSeO oxyselenide

Asep Ridwan Nugraha,*[a,b,c] Shaikh Shamim,[b] Andrei Novitskii,[b] Dedi,[c] Fainan Failamani,[d] Bambang Prijamboedi,[d] Takao Mori,[b] and Agustinus Agung Nugroho [d]

[a] *Physics Graduate Program, Institut Teknologi Bandung, Jl Ganesha 10, Bandung 40132, Indonesia.*
[b] *Research Center for Materials Nanoarchitectonics (MANA), National Institute for Materials Science (NIMS), Namiki 1-1, Tsukuba 305-0044, Japan.*
[c] *National Research and Innovation Agency (BRIN), Jl. Sangkuriang, Bandung 40135, Indonesia.*
[d] *Faculty of Mathematics and Natural Sciences (FMIPA), Institut Teknologi Bandung (ITB), Jl Ganesha 10, Bandung 40132, Indonesia.*
**Email: asep051@brin.go.id*

Abstract

BiCuSeO has intrinsically low electrical conductivity, high Seebeck coefficient and low thermal conductivity. Therefore, the improvement of BiCuSeO thermoelectric performance focuses on enhancing its electrical conductivity. In this study, we report one of the strategies to optimize carrier concentration by Cr doped on Cu site. After doping with Cr, enhanced electrical conductivity coupled with a moderate Seebeck coefficient leads to power factor of ~0.4 – 0.6 mW/mK^2 at 323 – 773 K. It is increased of ~4 – 6 times compared to pure BiCuSeO. Moreover, Cr doping reduces lattice thermal conductivity by ~21% as confirmed by both experimental result and Callaway model calculation. The analysis indicates that the lattice thermal conductivity can be reduced to 0.5 W m^{-1} K^{-1} at 773 K through the combined effect of point defect and phonon – electron scattering. The combination of optimized power factor and intrinsically low thermal conductivity result in high ZT_{max} and $ZT_{average}$. The ZT_{max} and $ZT_{average}$ values were obtained in the $BiCu_{0.96}Cr_{0.04}SeO$ sample of ~1.0 at 675 K and ~0.83 at 323 – 773 K, respectively. The high ZT of ~0.9 is realized over a broad temperature range from 473 to 773 K. This strategy makes BiCuSeO a promising candidate for medium temperature thermoelectric applications.

Keywords: BiCuSeO, point defect scattering, phonon – electron scattering, low lattice thermal conductivity, thermoelectric.

1. Introduction

The first layered oxyselenide $(BiO)Cu_{1-x}Se$ was synthesized by T.Ohtani et al. in 1997 during the rapid development of superconducting material [1]. It was reported that $(BiO)Cu_{1-x}Se$ are degenerate semiconductor with holes as dominant charge carrier. Two decades later, in 2010, Zhao et al. reported the thermoelectric performance of $Bi_{1-x}Sr_xCuSeO$ in medium temperature range. The highest ZT of 0.76 at 873K was achieved from the sample of 7.5% Sr-doped on Bi site [2]. Since then, the development of BiCuSeO for thermoelectric applications are still going on. High performance thermoelectric materials can lead to efficient power generation by their modules [T. Hendricks, T. Caillat, and T. Mori, "Keynote Review of Latest Advances in Thermoelectric Generation Materials, Devices, and Technologies 2022", Energies, 15, 7307 (2022). doi:10.3390/en15197307]. Pristine BiCuSeO exhibits low electrical conductivity, high Seebeck coefficient and low thermal conductivity [3]. Considering the high Seebeck coefficient and low thermal conductivity, several researches have been conducted to improve the thermoelectric performance of BiCuSeO through charge carrier optimization. The single-doped materials with monovalent (Ag [4], Na [5], and Cs [6]) ions or divalent (Pb [7], Mg [8], Ca [9], Ba [10], Cd [11], and Sn [12]) ions are well observed for doping in the Bi site. The monovalent or divalent ions can optimize the charge carrier concentrations from 10^{19} cm^{-3} to 10^{21} cm^{-3} which improved the electrical conductivity. Additionally, they can reduce the thermal conductivity by point defect scattering. The point defect scattering depends on the mass and strain fluctuation between monovalent or divalent ions with the host lattice. The large mass difference between Bi and monovalent or divalent ions yields a huge mass fluctuation that predominately contribute to reduce lattice thermal conductivity. However, the enhancement of thermoelectric performance achieved by single doped material on the Bi site has limitation due to a dramatic decrease in carrier mobility.

Several attempts have been made to introduce dual doping on the Bi site by using Pb/In [13], Pb/Ca [14], Pb/Na [15], Pb/Ba [16], Pb/In [17], on the Cu site by using Ba/Co [18], Pb/Ag [19], Ba/Ni [20], Pb/Fe [21], and on the Se sites by using

Ba/Te [22]. The majority of these materials utilized Pb as a dopant. It has been proven that doping on Bi site with Pb is very effective in increasing the carrier concentration of BiCuSeO. Since dopant Pb has electron configuration [Xe] $4f^{14}$ $5d^{10}$ $6s^2$ $6p^2$, the substitution of Pb on Bi [Xe] $4f^{14}$ $5d^{10}$ $6s^2$ $6p^3$ will produce more holes. Moreover, Pb doping introduces an additional peak near the Fermi level originated from delocalized lone-pair 6s orbital [7]. It can maintain moderate Seebeck coefficient by increasing the density of state effective mass. However, excessive use of heavy metal and toxic element such as Pb will cause environmental problems. Therefore, a new strategy is needed to improve the thermoelectric performance of BiCuSeO. To avoid the use of heavy and toxic metals, various transition metals have been used as dopants in Cu sites such as Mn [23], Fe [21], Co [24], Ni [20] and Zn [25]. The incorporation of Zn into the Cu site has been demonstrated to effectively enhance the carrier concentration by two orders of magnitude. Consequently, the maximum ZT of 0.9 was achieved at 873 K for $BiCu_{0.9}Zn_{0.1}SeO$, which is approximately 39% larger than that of the undoped BiCuSeO [25]. Similar to the enhancement observed in Zn doping, Ni doping in $Bi_{0.875}Ba_{0.125}Cu_{1-x}Ni_xSeO$ has also led to an increase in electrical conductivity, attributed to an enhanced carrier concentration. Furthermore, in this system, the magnetic ion of Ni has significantly improved the Seebeck coefficient. The maximum ZT of 0.97 was achieved for x = 0.15 at 923 K [20]. The influence of transition metal doping resulted in a remarkable enhancement of electrical conductivity while increasing the Seebeck coefficient, resulting in an improved power factor. This strategy seems promising due to the intrinsically low thermal conductivity of BiCuSeO. However, the thermoelectric performance of BiCuSeO by transition metal doping with lead-free material leaves some room for improvement.

In this report, we designed a single-doping at the single site-based experimental approach to produce high-performance BiCuSeO with lead-free material. We selected a transition metal element such as Cr as a dopant on the Cu site to improve the electronic transport properties. The Cr doping can modify the carrier concentration, which simultaneously increases the electrical conductivity while not deteriorating the Seebeck coefficient, leading to an enhanced power factor. The role of Cr doping is not only increasing the power factor but also decreasing lattice thermal conductivity. The decrease of lattice thermal conductivity is dominated by point defect and strong phonon – electron scattering. The ZT_{max} and $ZT_{average}$ have been achieved in $BiCu_{0.96}Cr_{0.04}SeO$ around ~1.0 at 675 K and ~0.83 at 323 – 773 K, respectively. To the best of our knowledge, it is the highest ZT_{max} and $ZT_{average}$ for single doping in BiCuSeO system.

2. Experimental details

Polycrystalline samples of $BiCu_{1-x}Cr_xSeO$ (x = 0, 0.02, 0.04, 0.06, and 0.08) were prepared by solid-state reaction followed with spark plasma sintering (SPS). The raw materials of nanopowder Bi_2O_3 (90 – 210 nm particle size, 2N, Sigma Aldrich), Bi (2N, Sigma Aldrich), Cu (2N, Sigma Aldrich), Cr (2N, Sigma Aldrich) and Se shot (2-6 mm, 5N, Alfa Aesar) were weighed according to stoichiometric ratio. The raw materials were mixed in agate pestle and mortar, then pressed into pellets under 20 MPa in a steel die. The pellets were sealed in quartz tubes under a vacuum (~10^{-3} Pa). Prior to use, the quartz tube had been baked in dry box for 1.5 h at 423 K to evaporate the volatile compounds such as alcohol and acetone. The ampoules were heated to 673 K at a rate of 2 K/min, then dwelled for 10 h to ensure that the reaction between chromium and other metals proceeded completely. Afterwards, the temperature slowly raised to 973 K at a rate of 1 K/min and held at this temperature for 20 h before cooling to room temperature naturally. The obtained ingots were hand-ground into fine powders and densified using SPS (SPS Syntax – 1080, Japan) at 973 K for 5 min under a uniaxial pressure of 50 MPa. Finally, the dense sintered pellets with a thickness of ~ 4 mm and a diameter of 10 mm were obtained.

The structural phases were identified using X-ray diffraction (XRD) Rigaku Mini-Flex, Japan, with Cu-Kα radiation (λ = 1.54060 Å). The obtained data were analyzed using GSAS [26]. The microstructure and compositional analysis of bulk sample were characterized by FE-SEM with EDS (SU-4800, Hitachi, Japan). Samples for EDS were embedded in a conductive resin and polished with standard metallographic procedures. The transport properties of electrical resistivity (ρ) and Seebeck coefficient (S) were measured in a low-pressure helium atmosphere on a commercial thermoelectric measurement system, ZEM-2 (Ulvac- Rico, Japan) from 323 K to 773 K. The typical dimensions of the electrical resistivity and Seebeck coefficient measurement are about 2 × 2 × 9 mm^3. The thermal diffusivity coefficient (D) was measured using laser flash method (LFA427, Netzsch, Germany) in same temperature range. The total thermal conductivity (κ) was calculated from the equation $\kappa = DC_pd$, where Cp is the specific heat calculated using Debye model, and d is the density measured by the Archimedes method. The electronic thermal conductivity (κ_E) is estimated using the Wiedemann-Franz law ($\kappa_E = L\sigma T$), where L was estimated by single parabolic band (SPB) model and acoustic phonon scattering (APS) [27]. The pieces of 8.4 mm × 8.4 mm × 0.5 mm were used for Hall coefficient (R_H) measurements under a reversible magnetic field of 0.52 T (ResiTest 8300DC, Tokyo, Japan). The Hall carrier concentration (n_H) and mobility (μ_H) were calculated using $n_H = 1/(eR_H)$ and $\mu_H = \sigma R_H$, respectively. The estimation of extended uncertainty measurement of electrical resistivity, Seebeck coefficient, thermal diffusivity, total thermal conductivity, and density are 5%, 5%, 5%, 10% and 2%, respectively. The combined uncertainty for all measurement involved in ZT determination is below 20%.

3. Result and discussions

3.1. Phase and microstructure

Figure 1 (a) shows the normalized XRD patterns of the $BiCu_{1-x}Cr_xSeO$ (x = 0; 0.02; 0.04; 0.06; 0.08) samples at room temperature. All the diffraction patterns of obtained $BiCu_{1-x}Cr_xSeO$ samples well be indexed to tetragonal BiCuSeO (PDF Card #67-00327) with P4/nmm space group. There are no additional peaks due to secondary phase in all samples indicating the high purity of our samples. Since the Cr content is very low, the peaks derived from the Cr were not found in the XRD patterns. However, the peaks were slightly shifted to the higher angle 2θ with the increase of doping content as shown in the Fig. 1 (b). These results indicate that the Cr element was successfully incorporated into the BiCuSeO lattice. The weighted profile factor (R_W), profile factor (R_F), GoF, and lattice constants refined from XRD data using by GSAS-II are shown in Table I. The lattice constant and volume of the $BiCu_{1-x}Cr_xSeO$ samples decrease with increase of doping content. The decrease of the lattice constants is related to the fact that the ionic radius of Cr^{2+} (73 pm) or Cr^{3+} (61 pm) are lower than that of Cu^{+} (74 pm) assuming with Cr have a mixed valence in the system. The lattice constants agree with experimental data obtained in Ref. [24] when giving Co-doped in the Cu site of BiCuSeO. The substitution of Cu^{+} by Cr^{2+} modifies the electronic charge carrier between layers become $(Bi_2O_2)^{(2-2x)+}$ and $((Cu_{1-x}Cr_x)_2Se_2)^{(2-2x)-}$ using simple electron count, respectively. Table 1 shows the bond length and angle of $d_{Cu\text{-}Se}$, $d_{Bi\text{-}O}$, $d_{Bi\text{-}Se}$, $\alpha_{Se\text{-}Cu\text{-}Se}$ and $\alpha_{Bi\text{-}O\text{-}Bi}$, respectively. A slight increase of the Cu/Cr-Se bond length can be observed, simultaneously with a slight increase of the distortion of the $CuSe_4$ tetrahedra. The massive change occurred at x = 0.04, where the Cr content influences the local environment of Cu in $((Cu_{1-x}Cr_x)_2Se_2)^{(2-2x)-}$ layer. Therefore, the angle of Se – Cu/Cr – Se decreases while the distances of Cu/Cr – Se and Bi – O increase. This effect leads to a reduction in the Coulombic attraction between layers and decrease the crystal volume. This is a similar mechanism with a decrease of the Bi – Se distance, which leads to a slight overlap of Bi and Se orbitals. This mechanism was also found in the $Bi_{1-x}Sr_xCuSeO$ [28] and $Bi_{0.94}Pb_{0.06}Cu_{1-x}Fe_xSeO$ series [21].

The texture refinement was fitted using 10th order spherical harmonics in GSAS-II for all samples compared with non-texture sample from ICDD. Figure 2 shows the fitted model compared with the diffraction intensity of the $BiCu_{1-x}Cr_xSeO$ (x = 0; 0.04) in (003) and (102) planes, respectively. The degree of preferred orientation of different crystal planes can be determined using Harris's analysis by calculating the texture coefficient as showed in eq (1)

$$P_{(h_ik_il_i)} = \frac{I_{(h_ik_il_i)}}{I_{o(h_ik_il_i)}} \left\{ \frac{1}{N} \sum_{i=1}^{N} \frac{I_{(h_ik_il_i)}}{I_{o(h_ik_il_i)}} \right\}^{-1} \quad (1)$$

where $P_{(h_ik_il_i)}$is the texture coefficient of the planes specified by Miller Indices (hkl), $I_{(h_ik_il_i)}$is the integrated intensity of texture sample, $I_{o\,(h_ik_il_i)}$is the intensity of non-texture sample and N is the number of diffractions. $P_{(h_ik_il_i)} = 0$ means that there is no orientation, $P_{(h_ik_il_i)} = 1$ means that the sample has random orientation and $P_{(h_ik_il_i)} > 1$ means that the sample is highly oriented. The increase of texture coefficient indicates that a higher degree of preferred orientation along a particular direction as compared with the non-texture sample. Figure 2 (inset) shows the degree of preferred orientation in (003) plane as a function of Cr doping. The texture analysis shows that the $BiCu_{0.96}Cr_{0.04}SeO$ is highly textured along (003) plane which 10 times higher than non-textured sample.

Figure 3 (a-b) displays the SEM images on the fractured surface of $BiCu_{1-x}Cr_xSeO$ with x = 0.00 and 0.04, respectively. It can be observed that the SEM image of pristine BiCuSeO exhibits a variety of shapes and sizes of crystals, whereas the $BiCu_{0.96}Cr_{0.04}SeO$ sample displays a lath-shaped crystal. The small dots on the images are identified as micropores, which are more prevalent in the pristine BiCuSeO sample than in the $BiCu_{0.96}Cr_{0.04}SeO$ sample. The average grain size of the pristine BiCuSeO and $BiCu_{0.96}Cr_{0.04}SeO$ samples is approximately 2.1 μm and 1.8 μm, respectively. Figure 4 (a-c) shows the SEM and EDX images on the polished surface of the $BiCu_{1-x}Cr_xSeO$ (x = 0.02;0.04; 0.08) samples. The Bi, Cu, and Se elements are homogeneously distributed in the BiCuSeO matrix. However, the $BiCu_{1-x}Cr_xSeO$ (x = 0.02; 0.04; 0.08) samples show an uneven distribution of Cr and O elements. The Cr and O elements are distributed randomly in the BiCuSeO matrix and some of them are agglomerated to form a chromium oxide. The point mapping on the Cr-rich area of the $BiCu_{0.96}Cr_{0.04}SeO$ indicate the presence of chromium oxide phases, CrO. Furthermore, the chromium oxide forms a composite in the BiCuSeO matrix at high Cr doped. Based on the results of SEM and EDX measurements, we estimate that the reaction occurring in this system can be expressed as follows:

$$Bi_2O_3 + Bi + 3xCr + 3Se + 3(1-x)Cu \rightarrow 3BiCu_{1-x}SeO_{1-x} + 3xCrO \quad (2)$$

and

$$Bi_2O_3 + Bi + 3xCr + 3Se + 3(1-x)Cu \rightarrow 3BiCu_{1-x}Cr_xSeO \quad (3)$$

Consistent with XRD measurement, it is also found that the CrO phases began to appear at x = 0.06, indicating that the solubility limit of Cr in the BiCuSeO matrix is less than x = 0.06. The solubility limit of $BiCu_{1-x}Cr_xSeO$ is lower than the $Bi_{1-x}Li_xCu_{1-x}Mn_xSeO$ [23] and $BiCu_{1-x}Co_xSeO$ [13], which are below 8% and 15%, respectively. The smaller solubility limit

of $BiCu_{1-x}Cr_xSeO$ is attributed to the larger ionic radius of Cr^{2+} (73 pm) in comparison to Mn^{2+} (67 pm) and Co^{2+} (65 pm), respectively.

3.2. Thermoelectric properties

The electrical conductivity (σ) for the $BiCu_{1-x}Cr_xSeO$ (x = 0; 0.02; 0.04; 0.06; 0.08) samples as a function of temperature is shown in Fig. 5 (a). The pristine BiCuSeO has a very low electrical conductivity as reported in various papers [5,9,29]. It has a continuous increasing tendency as the temperature rises. It indicates the degenerate semiconductor behavior. In addition, the $BiCu_{1-x}Cr_xSeO$ (x = 0.02; 0.04; 0.06; 0.08) samples show a significant enhance in electrical conductivity (~6 – 17 times) compared with the pristine BiCuSeO. Specially, the electrical conductivity of pristine BiCuSeO is ~3.44 S cm^{-1} at 473 K, while this value increase to ~52.46 S cm^{-1} in $BiCu_{0.94}Cr_{0.06}SeO$. The primary factor contributing to the increased conductivity of $BiCu_{1-x}Cr_xSeO$ (x = 0.02; 0.04; 0.06; 0.08) samples is the increase in carrier concentration in the system. Table 2 illustrates the carrier concentration and mobility of the $BiCu_{1-x}Cr_xSeO$ (x = 0; 0.02; 0.04; 0.06; 0.08) at room temperature. The substitution of Cu^+ by Cr^{2+} is theoretically expected to follow the equation, $Cr^{2+} \rightarrow Cr_{Cu}^{\bullet} + e'$. It was hypothesized that the substitution of Cu^+ by Cr^{2+} should produce more electrons than holes, resulting in a decrease in electrical conductivity and an increase in the Seebeck coefficient due to the charge carrier. However, the observed mechanism in our system does not align with this hypothesis. The probable explanation for this discrepancy lies in the possibility that Cu^+ is not fully substituted by Cr^{2+}. When the Cr doping concentration is low, the Cr^{2+} tends to form nano- to microscale precipitates of CrO. The CrO precipitates will create additional holes in the oxide layer due to the presence of oxygen vacancies and in the conducting layer due to a deficiency of copper. The additional holes increase the carrier concentration in the system. Upon further increase in Cr doping, the Cr^{2+} partially substitutes the unoccupied Cu^+, leading to the introduction of electrons. The CrO's tendency to provide holes is suppressed, which slightly decreased the carrier concentration. The introduction of Cr^{2+} in $BiCu_{1-x}Cr_xSeO$ can be illustrated by Eq. 4:

$$2(BiCu_{1-x}Cr_xSeO) = \left(Bi_2O_{2(1-x)}\right)^{2(1-x)+} + 2xh^+ + \left(Cu_{2(1-x)}Se_2\right)^{(2+x)-} + xV_{Cu}^- + 2xCrO + 2xh^+ \quad (4)$$

where V_{Cu}^- and h^+ are the Cu vacancy and the produced holes introduced by Cr doping, respectively.

Figure 5 (b) shows the temperature dependence of the Seebeck coefficient (S) of the $BiCu_{1-x}Cr_xSeO$ (x = 0; 0.02; 0.04; 0.06; 0.08) samples. The positive value of the Seebeck coefficient indicate the whole samples are *p*-type semiconductor. The pristine BiCuSeO has a high value of Seebeck coefficient of around 425 – 500 μV/K for a temperature range of 325 – 773 K. This value is higher than pristine BiCuSeO reported in the earlier studies [5,9,29]. The Seebeck coefficient decrease from ~ 484.5 μV/K in pristine BiCuSeO to ~ 305.4 μV/K in $BiCu_{0.94}Cr_{0.06}SeO$ at 473 K. The reduction in Seebeck coefficient consistent with the enhancement in electrical conductivity as the Cr doping increases. The Seebeck coefficient in doped sample decrease with raising temperature and reach a minimum value at 473 K. When T > 473 K it slightly increases monotonically, owing to the thermal activation of secondary phase of chromium oxide. In the context of ~~non-degenerate semiconductors~~, the effective mass (m^*) can be calculated by the following equation (5-7) based on experimental carrier concentration (n) and Seebeck coefficient (S), with the assumption of single parabolic band (SPB) model and acoustic phonon scattering (APS).

$$m^* = \frac{h^2}{2k_BT}\left(\frac{n}{4\pi F_{1/2(\eta)}}\right)^{2/3} \quad (5)$$

$$S = \pm\frac{k_B}{e}\left(\frac{(r+5/2)F_{r+3/2(\eta)}}{(r+3/2)F_{r+1/2(\eta)}} - \eta\right) \quad (6)$$

$$F_i(\eta) = \int_0^\infty \frac{x^i}{1+e^{x-\eta}}dx \quad (7)$$

Where $F_i(\eta)$ is the i-th order Fermi integral, $\eta = E_F/k_BT$ is the reduce Fermi energy, S is the Seebeck coefficient, k_B is the Boltzmann constant, e is the charge carrier, h is the reduces Plack constant, m^* is the carrier effective mass, n is the carrier concentration, and r is the scattering parameter which assumed as $-1/2$ for the acoustic phonon scattering near room temperature. The estimated of effective mass is presented in Table 2. The effective mass of $BiCu_{1-x}Cr_xSeO$ varies from ~3.9m_0 (m_0 is the free electron mass) to ~8.9m_0, indicating the multi-band behaviour in these doped samples. It is clear from Fig.5 (c) that the Seebeck coefficient decrease simultaneously with reduction of effective mass from ~4.7m_0 for x = 0 to ~4.1m_0 for x = 0.08 and increasing the carrier concentration from ~5.9×10^{18} for x = 0 to ~1.8 × 10^{19} for x = 0.08. The Pisarenko relationship of the Seebeck coefficient for non-degenerate semiconductors is fitted by equation (8). The results demonstrated that the dependence of S on n and m* for the $BiCu_{1-x}Cr_xSeO$ (x = 0; 0.02; 0.04; 0.06; 0.08) samples is in fair agreement with the theoretical description of the single parabolic band (SPB) model and acoustic phonon scattering (APS).

$$S = \pm\frac{k_B}{e}\left(\frac{5}{2} + r + ln\left[\frac{2(2\pi m^* k_B T)^{\frac{3}{2}}}{h^3 n}\right]\right) \quad (8)$$

The electronic transport properties of material are well explained by the weighted mobility. The weighted mobility calculated by equation 9 using the experimental data electrical conductivity and Seebeck coefficient proposed by J. Snyder which expressed as:[30]

$$\mu_w = \frac{3h^3\sigma}{8\pi e(2m_e k_B T)^{3/2}}\left[\frac{e^{\left[\frac{|S|}{k_B/e}-2\right]}}{1+e^{\left[-5\left(\frac{|S|}{k_B/e}-1\right)\right]}} + \frac{\frac{3}{\pi^2}\frac{|S|}{k_B/e}}{1+e^{\left[5\left(\frac{|S|}{k_B/e}-1\right)\right]}}\right] \quad (9)$$

where h, e, ρ, k_B, m_e, S, and T represent the Planck constant, the charge carrier, the experimental electrical resistivity in $m\Omega$ cm, the Boltzmann constant, the mass of electron, the experimental Seebeck coefficient, and the absolute temperature, respectively. Figure 5 (d) shows the weighted mobility of the $BiCu_{1-x}Cr_xSeO$ (x = 0, 0.02; 0.04; 0.06; 0.08) as a function of temperature. The μ_w of doped samples follow the $\sim T^{-1.5}$ tendency, indicates the domination of acoustic – phonon scattering in whole temperature region.

Figure 5 (e) shows the power factor of the $BiCu_{1-x}Cr_xSeO$ (x = 0; 0.02; 0.04; 0.06; 0.08) samples. The $BiCu_{0.96}Cr_{0.04}SeO$ sample shows the high electrical conductivity, while maintaining its Seebeck coefficient of around 350 – 425 μV/K in the whole temperature range. This makes the power factor (PF) of the $BiCu_{0.96}Cr_{0.04}SeO$ sample is the highest compared to all samples over the entire temperature range. The power factor of the $BiCu_{0.96}Cr_{0.04}SeO$ is around ~0.60 $mWm^{-1}K^{-2}$ at 473 K. This value is higher than that of Mg [29], Ca [9], Fe [23], Sb [31], La [32] and Pr [33] doped BiCuSeO. The power factor (PF) of the $BiCu_{1-x}Cr_xSeO$ decreases as the doping level increase further more than 0.04, which is attributed to the presence of secondary phase confirmed by SEM.

The total thermal conductivity of the pristine BiCuSeO sample decreases with increasing temperature, from ~1.09 $Wm^{-1}K^{-1}$ at 300 K to ~0.55 $Wm^{-1}K^{-1}$ at 773 K, as shown in Fig. 5 (f). The total thermal conductivity decreases with increased Cr doping fractions caused by multiple scattering factors. The maximum reduction in the total thermal conductivity is observed at x = 0.08, with a decrease of approximately 21.02%. In order to investigate the electronic and phonon contributions, we calculate the electronic thermal conductivity using Wiedermann – Franz relation, $k_E = L\sigma T$, where L was derived by equation 10 expressed as:

$$L = \left(\frac{k_B}{e}\right)^2\left(\frac{(r+\frac{7}{2})F_{r+\frac{5}{2}}(\eta)}{(r+\frac{3}{2})F_{r+\frac{1}{2}}(\eta)} - \left[\frac{(r+\frac{5}{2})F_{r+\frac{3}{2}}(\eta)}{(r+\frac{3}{2})F_{r+\frac{1}{2}}(\eta)}\right]^2\right) \quad (10)$$

with assumption of a single parabolic band (SPB) and acoustic phonon scattering (APS). Figure S5 (a-b) shows the Lorenz number and electronic thermal conductivity as a function of temperature. Based on the calculation, the electronic thermal conductivity of the $BiCu_{1-x}Cr_xSeO$ samples maintains a very low value over the temperature range. The maximum contribution of the electronic part to the total thermal conductivity is less than 2% for all samples. The lattice thermal conductivity decreases as the temperature decreases as shown in Fig.6 (a). It is hypothesized that the lattice thermal conductivity is reduced by point defect scattering through Cr doping. To understand the role of point defect in decreasing the lattice thermal conductivity, theoretical calculations are conducted using the Callaway model, which is defined as the ratio of the lattice thermal conductivity of a material containing a defect to that of the parent material [34,35] (see Supplementary Information).

$$\frac{\kappa_{lat}}{\kappa_{lat,p}} = \frac{tan^{-1}(u)}{u} \quad (11)$$

where κ_{lat}, $\kappa_{lat,p}$ are the lattice thermal conductivities of the defected and parent materials, respectively, and the parameter u is defined by:

$$u = \left(\frac{\pi^2\theta_D\Omega}{hv_a^2}\kappa_{lat,p}\Gamma\right)^{\frac{1}{2}} \quad (12)$$

where h, Ω, v_a and θ_D stand for the Planck constant, average volume per atom, lattice sound velocity (v_a = 2107 m/s) [9], and the Debye temperature (θ_D = 243 K) [36]. The disorder parameter $\Gamma = \Gamma_M + \varepsilon\Gamma_{SF}$ is calculated by Abeles and Slack model which includes both mass fluctuation (Γ_M) and strain field fluctuation between Cr – Cu atom (Γ_{SF}) [37,38]. In our system, the adjustable parameter ε is approximately 170, obtained from the fitting between the model and experimental data. The disorder parameter Γ varies depending on the fractional occupation of the Cr on the Cu site. The disorder parameter and the difference between the calculated and measured values are listed in Table S2, respectively. The result reveals that the calculated lattice thermal conductivity at room temperature agrees with the measured value, which is significantly lower than the uncertainty measurement, as shown in the Fig.6 (a)(inset). However, the reduction in lattice thermal conductivity in Cr-doped samples as a function of temperature remains to be investigated. Several factors may contribute to decrease in lattice

thermal conductivity, such as Umklapp process, point defect, grain boundary and phonon – electron scattering. To elucidate the contribution of each scattering mechanisms as a function of temperature, the Callaway model was employed to evaluate the lattice thermal conductivity [39]. Here, κ_L can be calculated from the following equation (13-14):

$$\kappa_L = \frac{k_B}{2\pi^2 v_s}\left(\frac{k_B T}{\hbar}\right)^3 \int_0^{\theta_D} \tau_{tot} \frac{x^4 e^x}{e^x - 1} dx \quad (13)$$

$$\tau_{tot} = \tau_U + \tau_{PD} + \tau_{GB} + \tau_{PE} \quad (14)$$

where τ_{tot} is the total relaxation time. The detailed calculations and fitting parameters for this model are provided in the Supplementary Information. The analysis was restricted to data below 600 K to minimize the bipolar effect. As depicted in Fig. 6(b), the calculation of the lattice thermal conductivity (κ_L) using the Callaway model shows good agreement with the measured values. This model underscores the significant role of various scattering mechanisms in enhancing phonon scattering. The contributions of each scattering mechanism to the reduction of lattice thermal conductivity are illustrated in Fig. 6(c). The solid light blue line, dashed red line, dashed blue line, and dashed green line represent the contributions from the Umklapp process (U), Umklapp process and point defect scattering (U+PD), Umklapp process, point defect and phonon-electron scattering (U+PD+PE), and Umklapp process, point defect, phonon-electron, and grain boundary scattering (U+PD+PE+GB), respectively. As expected from the fractured samples observed in SEM measurements, grain boundary scattering (GB) does not significantly reduce lattice thermal conductivity due to the large grain size in both pristine and doped samples. Large grain sizes are less effective in scattering low – frequency phonons compared to nano grain size. Figure 6 (c) further compares the model excluding phonon-electron scattering (U+PD) with the model including it (U+PD+PE). The analysis indicates that the Umklapp process and point defect scattering contribute only ~7.24% to the reduction of lattice thermal conductivity. When phonon – electron scattering is included, the calculated κ_L decreases by approximately 20.39%, achieving a good match between theoretical and experimental data. Phonon – electron scattering significantly contributes (~13.15%) to phonon scattering across a wide frequency range. Phonon – electron scattering disrupts the coherent propagation of phonons. Each scattering event can change the direction and energy of phonons, effectively hindering their ability to carry heat in a straight line through the lattice, resulting in a lower lattice thermal conductivity.

The figure of merit (ZT) of the $BiCu_{1-x}Cr_xSeO$ (x = 0.02; 0.04; 0.06; 0.08) samples as a function of temperature are shown in Fig 8 (a). The $BiCu_{0.96}Cr_{0.04}SeO$ and $BiCu_{0.94}Cr_{0.06}SeO$ samples have a ZT of about ~0.9 in the temperature range of 473 – 773 K. This value increases by about ~ 130 – 150 % as compared to pristine BiCuSeO. The ZT_{max} was obtained in the $BiCu_{0.96}Cr_{0.04}SeO$ sample with a value of ~1.0 at 675 K. If we compare with several doping elements by single-doped method such as Pb [7], Ba [10], Cd [11], Ca [9], Sm [40], Sr [41], Na [42], La [32], Mg [29] and dual-doped method such as Pb/Fe [21] and Pb/Ca [14], our result show a moderate value among the BiCuSeO system. The achieved ZT_{max} is obtained in the low temperature region. It is lower than the other results which usually obtain the ZT_{max} above 800 K. The highest ZT_{max} is observed for the BiCuSeO system with the Pb/Fe double doping method at the Bi/Cu site with a value of ~1.5 at 873 K [21]. Furthermore, Cr doping can significantly increase the $ZT_{average}$, which plays an important role in the applications. The calculated $ZT_{average}$ of the $BiCu_{0.96}Cr_{0.04}SeO$ sample is approximately 0.83 in the temperature range of 323 – 773 K. It is the highest value among the single-doped system. This value can compete with the Pb/Fe and Pb/Ca dual-doped systems, where both systems use heavy metals and toxic materials. In contrast, our method only uses Cr single-doped, which is more environmentally friendly.

Conclusions

In conclusion, the synthesis of $BiCu_{1-x}Cr_xSeO$ compounds with x = 0, 0.02, 0.04, 0.06, and 0.08 was successfully accomplished using the SSR+SPS method. The $BiCu_{0.96}Cr_{0.04}SeO$ sample exhibited maximum and average figure of merit, ZT_{max} and $ZT_{average}$, of approximately 1.0 at 675 K and 0.83 over the temperature range of 323–773 K, respectively. These values represent enhancements of about 150% and 330%, respectively, compared to the pristine BiCuSeO. The observed improvement in ZT is attributed to two main factors. Firstly, the increased charge carrier concentration improved electrical conductivity, as the substitution of Cr atoms generated additional holes in the oxide layer due to oxygen vacancies and in the conducting layer due to copper deficiency. Secondly, the reduction in lattice thermal conductivity was achieved through point defect scattering and phonon-electron scattering. The disparity in mass and strain fields between Cr and Cu atoms led to increased point defect scattering, while phonon-electron interactions significantly enhanced phonon scattering across a wide frequency range, thereby reducing lattice thermal conductivity. Our results demonstrate a remarkable improvement in both ZT_{max} and $ZT_{average}$ through single doping, achieving a ZT of approximately 0.9 in the low-temperature region of 473–773 K. This strategy makes $BiCu_{1-x}Cr_xSeO$ a promising candidate for medium-temperature thermoelectric applications.

Acknowledgements

This work was supported by The Indonesia Endowment Fund for Education (LPDP), Indonesia and International Cooperative Graduate Program (ICGP), NIMS- Japan. The authors also gratefully acknowledge the facilities, scientific and technical support of Advanced Characterization Laboratories, National Research and Innovation Agency (BRIN), E-Layanan Sains, Bandung, Indonesia.

References

[1] T. Ohtani, Y. Tachibana, Y. Fujii, Electrical properties of layered copper oxyselenides (BiO)Cu1 − xSe and (Bi1 − xSrx)OCuSe, J Alloys Compd 262–263 (1997) 175–179. https://doi.org/10.1016/S0925-8388(97)00375-7.

[2] L.D. Zhao, D. Berardan, Y.L. Pei, C. Byl, L. Pinsard-Gaudart, N. Dragoe, Bi1−xSrxCuSeO oxyselenides as promising thermoelectric materials, Appl Phys Lett 97 (2010) 092118. https://doi.org/10.1063/1.3485050.

[3] L.D. Zhao, J. He, D. Berardan, Y. Lin, J.F. Li, C.W. Nan, N. Dragoe, BiCuSeO oxyselenides: new promising thermoelectric materials, Energy Environ Sci 7 (2014) 2900–2924. https://doi.org/10.1039/C4EE00997E.

[4] Y. chun Liu, Y. hua Zheng, B. Zhan, K. Chen, S. Butt, B. Zhang, Y. hua Lin, Influence of Ag doping on thermoelectric properties of BiCuSeO, J Eur Ceram Soc 35 (2015) 845–849. https://doi.org/10.1016/J.JEURCERAMSOC.2014.09.015.

[5] J. Li, J. Sui, Y. Pei, X. Meng, D. Berardan, N. Dragoe, W. Cai, L.D. Zhao, The roles of Na doping in BiCuSeO oxyselenides as a thermoelectric material, J Mater Chem A Mater 2 (2014) 4903–4906. https://doi.org/10.1039/C3TA14532H.

[6] A. Achour, K. Chen, M.J. Reece, Z. Huang, Enhanced thermoelectric performance of Cs doped BiCuSeO prepared through eco-friendly flux synthesis, J Alloys Compd 735 (2018) 861–869. https://doi.org/10.1016/J.JALLCOM.2017.11.104.

[7] J.-L. Lan, Y.-C. Liu, B. Zhan, Y.-H. Lin, B. Zhang, X. Yuan, W. Zhang, W. Xu, C.-W. Nan, Enhanced Thermoelectric Properties of Pb-doped BiCuSeO Ceramics, Advanced Materials 25 (2013) 5086–5090. https://doi.org/10.1002/adma.201301675.

[8] J.-L. Lan, B. Zhan, Y.-C. Liu, B. Zheng, Y. Liu, Y.-H. Lin, C.-W. Nan, Doping for higher thermoelectric properties in p-type BiCuSeO oxyselenide, Appl Phys Lett 102 (2013) 123905. https://doi.org/10.1063/1.4799643.

[9] Y.-L. Pei, J. He, J.-F. Li, F. Li, Q. Liu, W. Pan, C. Barreteau, D. Berardan, N. Dragoe, L.-D. Zhao, High thermoelectric performance of oxyselenides: intrinsically low thermal conductivity of Ca-doped BiCuSeO, NPG Asia Mater (2013). https://doi.org/10.1038/am.2013.15.

[10] J. Li, J. Sui, Y. Pei, C. Barreteau, D. Berardan, N. Dragoe, W. Cai, J. He, L.D. Zhao, A high thermoelectric figure of merit ZT > 1 in Ba heavily doped BiCuSeO oxyselenides, Energy Environ Sci 5 (2012) 8543–8547. https://doi.org/10.1039/C2EE22622G.

[11] M.U. Farooq, S. Butt, K. Gao, Y. Zhu, X. Sun, X. Pang, S.U. Khan, F. Mohmed, A. Mahmood, N. Mahmood, W. Xu, Cd-doping a facile approach for better thermoelectric transport properties of BiCuSeO oxyselenides, RSC Adv 6 (2016) 33789–33797. https://doi.org/10.1039/C6RA01686C.

[12] Y. Yang, X. Liu, X. Liang, Thermoelectric properties of Bi1−xSnxCuSeO solid solutions, Dalton Transactions 46 (2017) 2510–2515. https://doi.org/10.1039/C6DT04885D.

[13] F. Li, M. Ruan, Y. Chen, W. Wang, J. Luo, Z. Zheng, P. Fan, Enhanced thermoelectric properties of polycrystalline BiCuSeO via dual-doping in Bi sites, Inorg Chem Front 6 (2019) 799–807. https://doi.org/10.1039/C8QI01402G.

[14] Y. Liu, L.-D. Zhao, Y. Zhu, Y. Liu, F. Li, M. Yu, D.-B. Liu, W. Xu, Y.-H. Lin, C.-W. Nan, Synergistically Optimizing Electrical and Thermal Transport Properties of BiCuSeO via a Dual-Doping Approach, Adv Energy Mater 6 (2016) 1502423. https://doi.org/https://doi.org/10.1002/aenm.201502423.

[15] S. Das, S.M. Valiyaveettil, K.-H. Chen, S. Suwas, R. Chandra Mallik, Thermoelectric properties of Pb and Na dual doped BiCuSeO, AIP Adv 9 (2019) 015025. https://doi.org/10.1063/1.5066296.

[16] B. Feng, G. Li, Z. Pan, Y. Hou, C. Zhang, C. Jiang, J. Hu, Q. Xiang, Y. Li, Z. He, X. Fan, Effect of Ba and Pb dual doping on the thermoelectric properties of BiCuSeO ceramics, Mater Lett 217 (2018) 189–193. https://doi.org/10.1016/j.matlet.2018.01.074.

[17] Y.-X. Chen, W. Qin, A. Mansoor, A. Abbas, F. Li, G. Liang, P. Fan, M.U. Muzaffar, B. Jabar, Z. Ge, Z. Zheng, Realizing high thermoelectric performance via selective resonant doping in oxyselenide BiCuSeO, Nano Res 16 (2023) 1679–1687. https://doi.org/10.1007/s12274-022-4810-8.

[18] Q. Wen, H. Zhang, F. Xu, L. Liu, Z. Wang, G. Tang, Enhanced thermoelectric performance of BiCuSeO via dual-doping in both Bi and Cu sites, J Alloys Compd 711 (2017) 434–439. https://doi.org/https://doi.org/10.1016/j.jallcom.2017.04.031.

[19] F. Li, Z. Zheng, Y. Chang, M. Ruan, Z. Ge, Y. Chen, P. Fan, Synergetic Tuning of the Electrical and Thermal Transport Properties via Pb/Ag Dual Doping in BiCuSeO, ACS Appl Mater Interfaces 11 (2019) 45737–45745. https://doi.org/10.1021/acsami.9b16723.

[20] Q. Wen, C. Chang, L. Pan, X. Li, T. Yang, H. Guo, Z. Wang, J. Zhang, F. Xu, Z. Zhang, G. Tang, Enhanced thermoelectric performance of BiCuSeO by increasing Seebeck coefficient through magnetic ion incorporation, J Mater Chem A Mater 5 (2017) 13392–13399. https://doi.org/10.1039/C7TA03659K.

[21] L. Pan, Y. Lang, L. Zhao, D. Berardan, E. Amzallag, C. Xu, Y. Gu, C. Chen, L.D. Zhao, X. Shen, Y. Lyu, C. Lu, Y. Wang, Realization of n-type and enhanced thermoelectric performance of p-type BiCuSeO by controlled iron incorporation, J Mater Chem A Mater 6 (2018) 13340–13349. https://doi.org/10.1039/C8TA03521K.

[22] B. Feng, G. Li, Z. Pan, X. Hu, P. Liu, Z. He, Y. Li, X. Fan, Enhanced thermoelectric performance in BiCuSeO oxyselenides via Ba/Te dual-site substitution and 3D modulation doping, J Solid State Chem 266 (2018) 297–303. https://doi.org/https://doi.org/10.1016/j.jssc.2018.07.034.

[23] J. Tang, R. Xu, J. Zhang, D. Li, W. Zhou, X. Li, Z. Wang, F. Xu, G. Tang, G. Chen, Light Element Doping and Introducing Spin Entropy: An Effective Strategy for Enhancement of Thermoelectric Properties in BiCuSeO, ACS Appl Mater Interfaces 11 (2019) 15543–15551. https://doi.org/10.1021/acsami.9b00958.

[24] S. Tan, C. Gao, C. Wang, Y. Sun, Q. Jing, Q. Meng, T. Zhou, J. Ren, Realization of n-type BiCuSeO through Co doping, Solid State Sci 98 (2019) 106019. https://doi.org/10.1016/J.SOLIDSTATESCIENCES.2019.106019.

[25] G.-K. Ren, S. Butt, Y.-C. Liu, J.-L. Lan, Y.-H. Lin, C.-W. Nan, F. Fu, X.-F. Tang, Enhanced thermoelectric performance of Zn-doped oxyselenides: BiCu1−xZnxSeO, Physica Status Solidi (a) 211 (2014) 2616–2620. https://doi.org/10.1002/pssa.201431347.

[26] B.H. Toby, R.B. Von Dreele, GSAS-II: the genesis of a modern open-source all purpose crystallography software package, J Appl Crystallogr 46 (2013) 544–549. https://doi.org/10.1107/S0021889813003531.

[27] H.-S. Kim, Z.M. Gibbs, Y. Tang, H. Wang, G.J. Snyder, Characterization of Lorenz number with Seebeck coefficient measurement, APL Mater 3 (2015) 41506. https://doi.org/10.1063/1.4908244.

[28] C. Barreteau, D. Bérardan, E. Amzallag, L.D. Zhao, N. Dragoe, Structural and electronic transport properties in Sr-doped BiCuSeO, Chemistry of Materials 24 (2012) 3168–3178. https://doi.org/10.1021/cm301492z.

[29] J. Li, J. Sui, C. Barreteau, D. Berardan, N. Dragoe, W. Cai, Y. Pei, L.D. Zhao, Thermoelectric properties of Mg doped p-type BiCuSeO oxyselenides, J Alloys Compd 551 (2013) 649–653. https://doi.org/10.1016/J.JALLCOM.2012.10.160.

[30] G.J. Snyder, A.H. Snyder, M. Wood, R. Gurunathan, B.H. Snyder, C. Niu, Weighted Mobility, Advanced Materials 32 (2020) 2001537. https://doi.org/https://doi.org/10.1002/adma.202001537.

[31] B. Feng, G. Li, Y. Hou, C. Zhang, C. Jiang, J. Hu, Q. Xiang, Y. Li, Z. He, X. Fan, Enhanced thermoelectric properties of Sb-doped BiCuSeO due to decreased band gap, J Alloys Compd 712 (2017) 386–393. https://doi.org/10.1016/J.JALLCOM.2017.04.121.

[32] Y. Liu, J. Ding, B. Xu, J. Lan, Y. Zheng, B. Zhan, B. Zhang, Y. Lin, C. Nan, Enhanced thermoelectric performance of La-doped BiCuSeO by tuning band structure, Appl Phys Lett 106 (2015) 233903. https://doi.org/10.1063/1.4922492.

[33] A. Novitskii, I. Serhiienko, S. Novikov, Y. Ashim, M. Zheleznyi, K. Kuskov, D. Pankratova, P. Konstantinov, A. Voronin, O.A. Tretiakov, T. Inerbaev, A. Burkov, V. Khovaylo, Influence of Bi Substitution with Rare-Earth Elements on the Transport Properties of BiCuSeO Oxyselenides, ACS Appl Energy Mater 5 (2022) 7830–7841. https://doi.org/10.1021/acsaem.2c01375.

[34] J. Callaway, H.C. von Baeyer, Effect of Point Imperfections on Lattice Thermal Conductivity, Physical Review 120 (1960) 1149–1154. https://doi.org/10.1103/PhysRev.120.1149.

[35] C.L. Wan, W. Pan, Q. Xu, Y.X. Qin, J.D. Wang, Z.X. Qu, M.H. Fang, Effect of point defects on the thermal transport properties of (LaxGd1- x)2Zr2O7 : Experiment and theoretical model, Phys Rev B 74 (2006) 144109. https://doi.org/10.1103/PhysRevB.74.144109.

[36] L. Pan, D. Bérardan, L. Zhao, C. Barreteau, N. Dragoe, Influence of Pb doping on the electrical transport properties of BiCuSeO, Appl Phys Lett 102 (2013). https://doi.org/10.1063/1.4775593/975500.

[37] G.A. Slack, Effect of Isotopes on Low-Temperature Thermal Conductivity, Physical Review 105 (1957) 829–831. https://doi.org/10.1103/PhysRev.105.829.

[38] R. Gurunathan, R. Hanus, M. Dylla, A. Katre, G.J. Snyder, Analytical Models of Phonon--Point-Defect Scattering, Phys Rev Appl 13 (2020) 34011. https://doi.org/10.1103/PhysRevApplied.13.034011.

[39] J. Callaway, Model for Lattice Thermal Conductivity at Low Temperatures, Physical Review 113 (1959) 1046–1051. https://doi.org/10.1103/PhysRev.113.1046.

[40] B. Feng, X. Jiang, Z. Pan, L. Hu, X. Hu, P. Liu, Y. Ren, G. Li, Y. Li, X. Fan, Preparation, Structure, and enhanced thermoelectric properties of Sm-doped BiCuSeO oxyselenide, Mater Des 185 (2020) 108263. https://doi.org/https://doi.org/10.1016/j.matdes.2019.108263.

[41] L.D. Zhao, D. Berardan, Y.L. Pei, C. Byl, L. Pinsard-Gaudart, N. Dragoe, Bi1-x Srx CuSeO oxyselenides as

promising thermoelectric materials, Appl Phys Lett 97 (2010). https://doi.org/10.1063/1.3485050.
[42] J. Le Lan, C. Deng, W. Ma, G.K. Ren, Y.H. Lin, X. Yang, Ultra-fast synthesis and high thermoelectric properties of heavy sodium doped BiCuSeO, J Alloys Compd 708 (2017) 955–960. https://doi.org/10.1016/J.JALLCOM.2017.02.290.

Table captions

Table 1: Lattice parameters, local structures (bond distance and angle), and atomic positions obtained from Rietveld analysis using GSAS-II

x	*a* (Å)	*c* (Å)	Vol. (Å)^3	GoF	R_W	R_F	*d* (Cu-Se) (Å)	*d* (Bi-O) (Å)	*d* (Bi-Se) (Å)	Angle (°) (Se-Cu-Se)	Angle (°) (Bi-O-Bi)
0.00	3.9296(3)*	8.9296(7)	137.89(3)	1.17	5.68	4.55	2.516(0)	2.331(0)	3.226(0)	102.66(0)	114.87(0)
0.02	3.9295(2)	8.9299(7)	137.89(3)	1.36	6.42	2.49	2.517(0)	2.331(0)	3.226(0)	102.62(0)	114.93(0)
0.04	3.9293(4)	8.9297(1)	137.87(3)	1.58	6.97	4.11	2.519(0)	2.332(0)	3.222(0)	102.50(0)	114.78(0)
0.06	3.9287(2)	8.9279(7)	137.80(3)	1.34	6.38	3.82	2.517(0)	2.331(0)	3.224(0)	102.57(0)	114.88(0)
0.08	3.9288(6)	8.9299(5)	137.84(3)	1.31	6.24	2.55	2.515(0)	2.330(0)	3.227(0)	102.72(0)	114.94(0)

Phase	*BiCuSeO*	*$BiCu_{0.98}Cr_{0.02}SeO$*	*$BiCu_{0.96}Cr_{0.04}SeO$*	*$BiCu_{0.94}Cr_{0.06}SeO$*	*$BiCu_{0.92}Cr_{0.08}SeO$*
Atomic Positions					
Bi					
x	0.25	0.25	0.25	0.25	0.25
y	0.25	0.25	0.25	0.25	0.25
z	0.140478	0.139951	0.140776	0.140472	0.140161
Cu					
X	0.75	0.75	0.75	0.75	0.75
Y	0.25	0.25	0.25	0.25	0.25
Z	0.5	0.5	0.5	0.5	0.5
Se					
X	0.25	0.25	0.25	0.25	0.25
Y	0.25	0.25	0.25	0.25	0.25
Z	0.676039	0.675982	0.676661	0.676678	0.675802
O					
X	0.75	0.75	0.75	0.75	0.75
Y	0.25	0.25	0.25	0.25	0.25
Z	0	0	0	0	0
Cr					
x	-	0.75	0.75	0.75	0.75
y	-	0.25	0.25	0.25	0.25
z	-	0.5	0.5	0.5	0.5

*Standard deviations are given in parentheses and refer to the estimated errors in the least significant units.

Table 2. Carrier concentration, carrier mobility, effective mass, and density of the $BiCu_{1-x}Cr_xSeO$ (x = 0; 0.02; 0.04; 0.06; 0.08) samples at room temperature.

samples	n (10^{19} cm^{-3})	μ (cm^2 V^{-1} S^{-1})	$m^*(m_0)$	ρ (g/cm^3)
x = 0	0.596	4.979	4.726	8.453
x = 0.02	1.298	1.412	3.909	8.454
x = 0.04	5.683	0.223	8.905	8.459
x = 0.06	2.128	0.293	4.420	8.673
x = 0.08	1.846	0.338	4.174	8.421

Figure captions

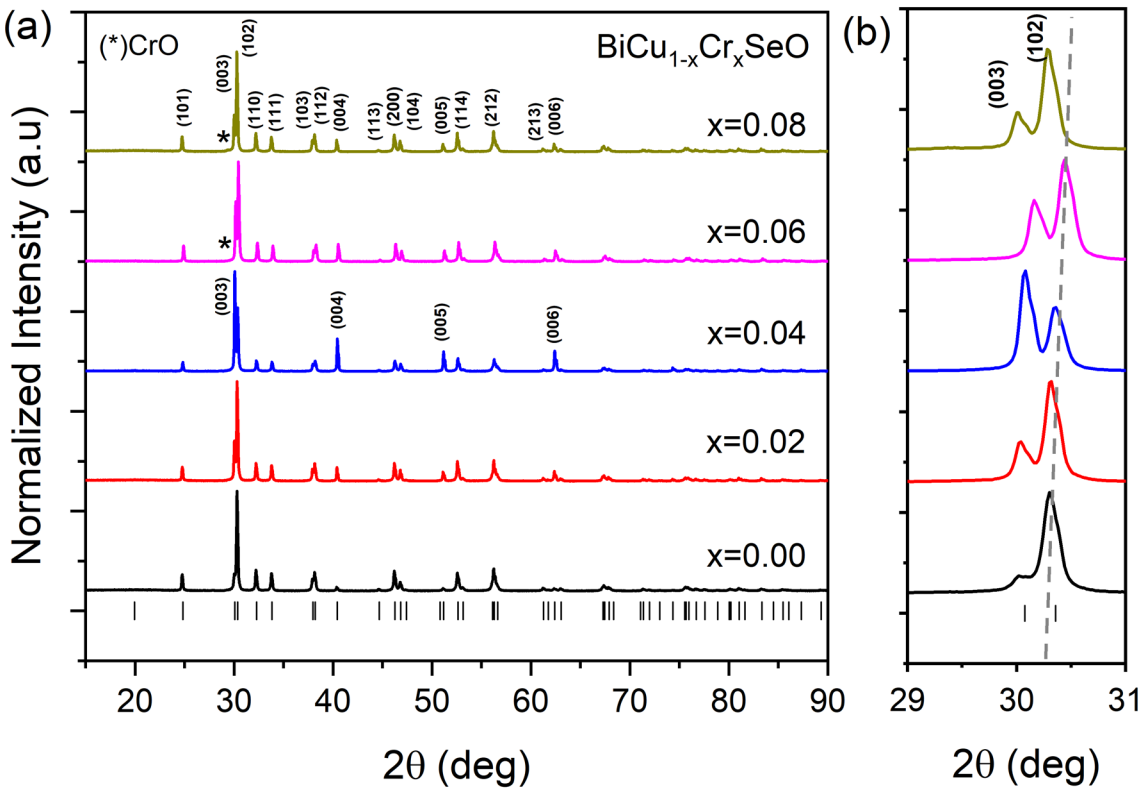

Figure 1. (a). The XRD patterns of the $BiCu_{1-x}Cr_xSeO$ (x = 0; 0.02; 0.04; 0.06; 0.08) samples at room temperature (b). The enlarged peaks at 2θ between 29° - 31°

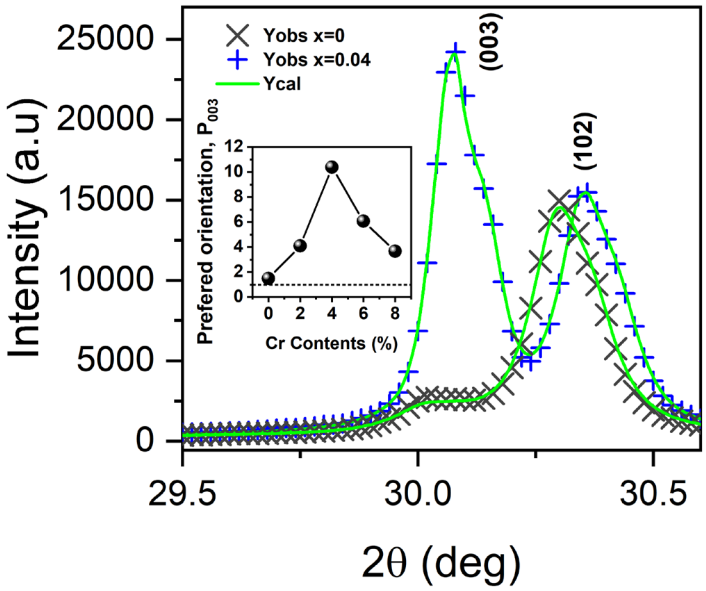

Figure 2. Texture refinement using spherical harmonic in GSAS-II. Degree of preferred orientation in 003 plane (inset)

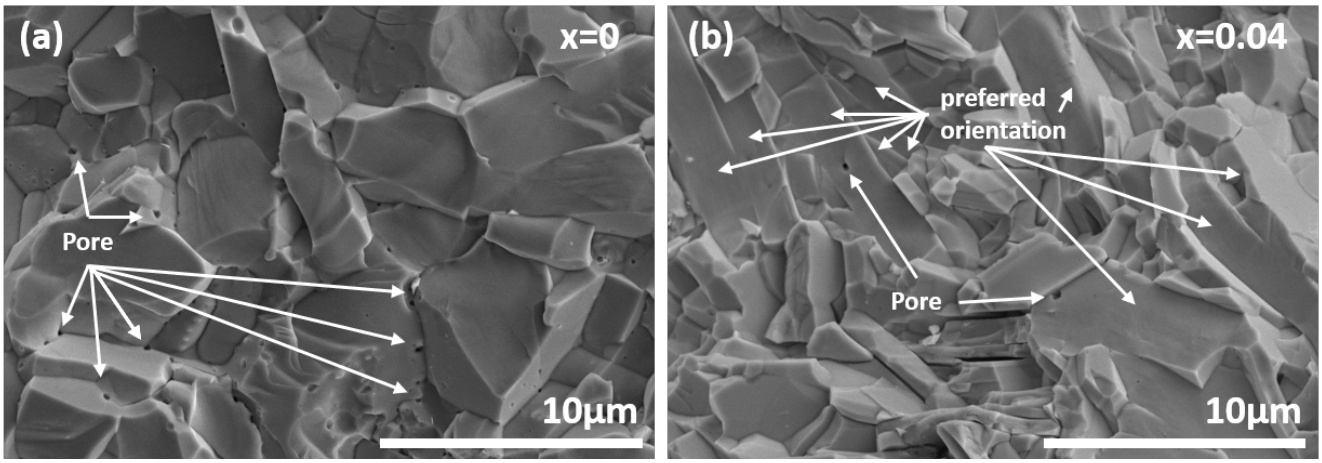

Figure 3. The SEM images of the fractured sample of $BiCu_{1-x}Cr_xSeO$ (a) $x = 0$ (b) $x = 0.04$ samples

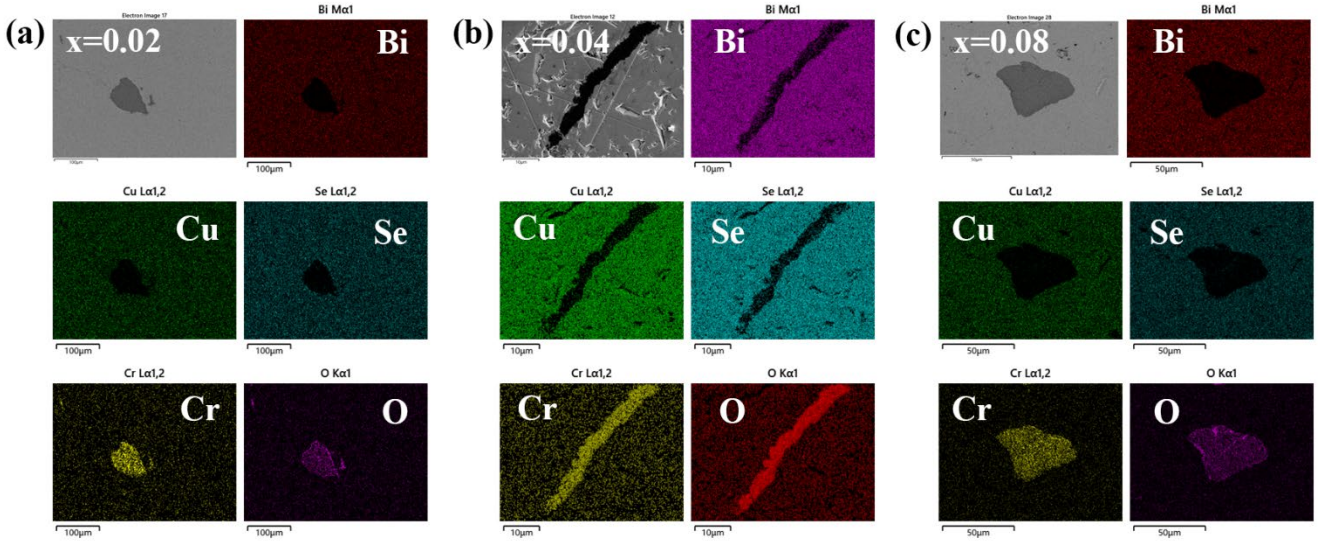

Figure 4. The elemental mapping of polished surface of the $BiCu_{1-x}Cr_xSeO$ (a) $x = 0.02$, (b) $x = 0.04$, and (c) $x = 0.08$

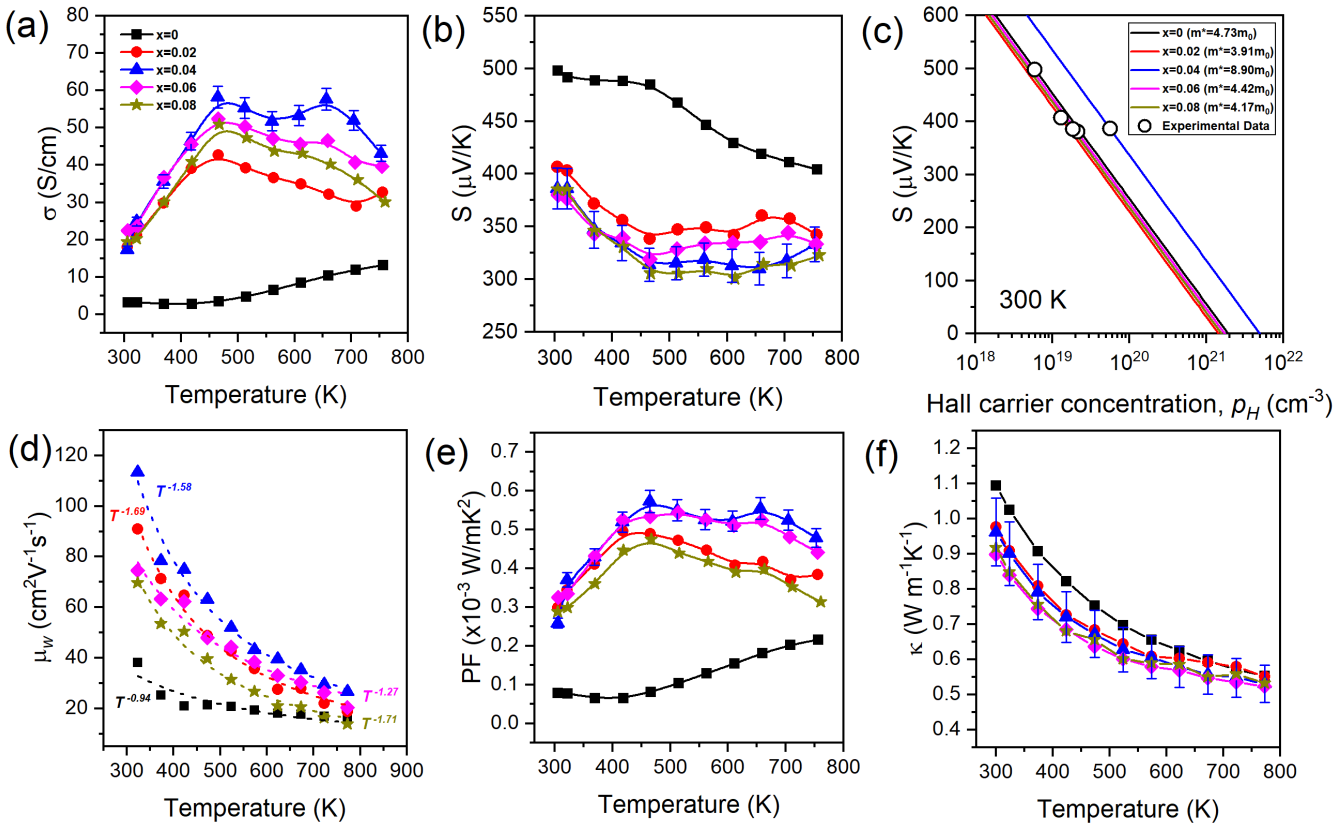

Figure 5. Thermoelectric properties as a function of temperature of the $BiCu_{1-x}Cr_xSeO$ (x = 0; 0.02; 0.04; 0.06; 0.08) samples, (a) Electrical conductivity, (b) Seebeck coefficient, (c) Pisarenko plot for non-degenerate semiconductor at 300 K, (d) The weighted mobility (the dash-line represent the trend of $\mu_w \propto T^{-n}$), (e) Power factor (PF), and (f) Total thermal conductivity.

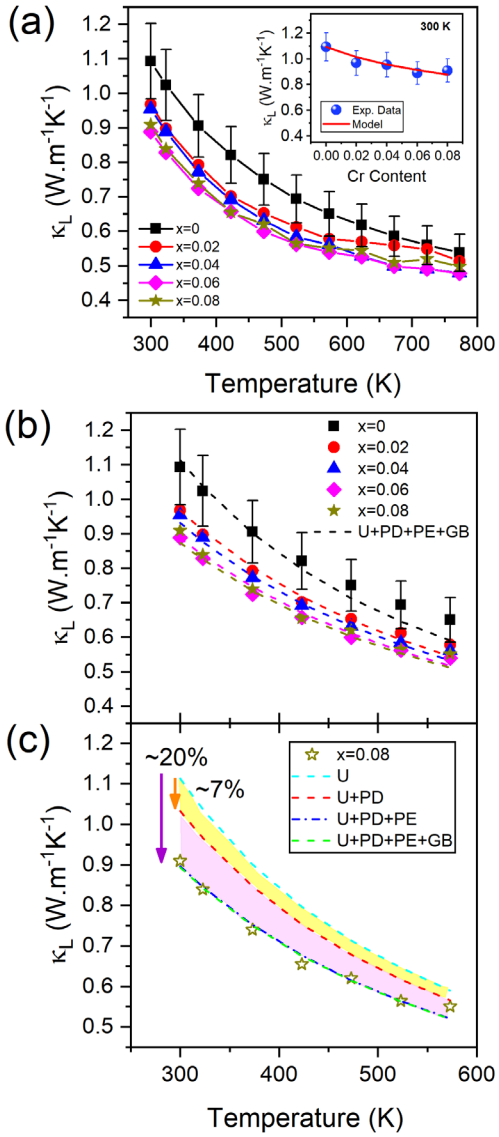

Figure 6. (a). The temperature dependent of κ_L for the $BiCu_{1-x}Cr_xSeO$ samples (symbols). (inset) A comparison of the experimental and the calculated lattice thermal conductivity at 300 K. (b) The dash line showing the prediction of κ_L using the Callaway model with different scattering mechanism. (c). The contribution of Umklapp process scattering (U), point defect scattering (PD), phonon – electron scattering (PE) and grain boundary scattering (GB) for the $BiCu_{1-x}Cr_xSeO$ ($x = 0.08$) samples.

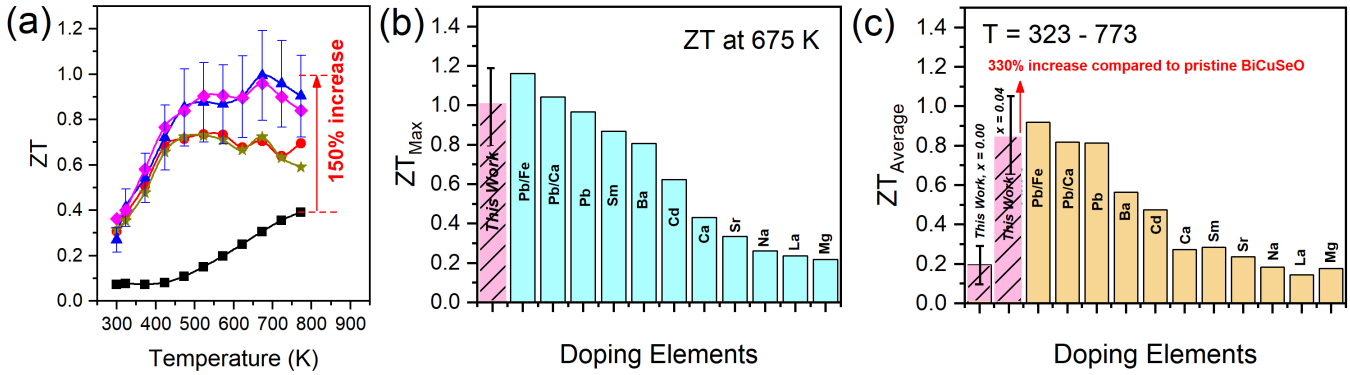

Figure 7. (a) The ZT as a function of temperature, (b) The comparison of ZT_{max} at 675 K, (c) The comparison of $ZT_{average}$ in the temperature range of 323 – 773 K compared with several doping elements from earlier studies

Supporting information:

High-ZT from optimized carrier concentration and electron – phonon interaction of Cr-doped BiCuSeO oxyselenide

Asep Ridwan Nugraha,*[a,b,c] Shaikh Shamim,[b] Andrei Novitskii,[b] Dedi,[c] Fainan Failamani,[d] Bambang Prijamboedi,[d] Takao Mori,[b] and Agustinus Agung Nugroho [d]

[a] *Physics Graduate Program, Institut Teknologi Bandung, Jl Ganesha 10, Bandung 40132, Indonesia.*
[b] *Research Center for Materials Nanoarchitectonics (MANA), National Institute for Materials Science (NIMS), Namiki 1-1, Tsukuba 305-0044, Japan.*
[c] *National Research and Innovation Agency (BRIN), Jl. Sangkuriang, Bandung 40135, Indonesia.*
[d] *Faculty of Mathematics and Natural Sciences (FMIPA), Institut Teknologi Bandung (ITB), Jl Ganesha 10, Bandung 40132, Indonesia.*
**Email: asep051@brin.go.id*

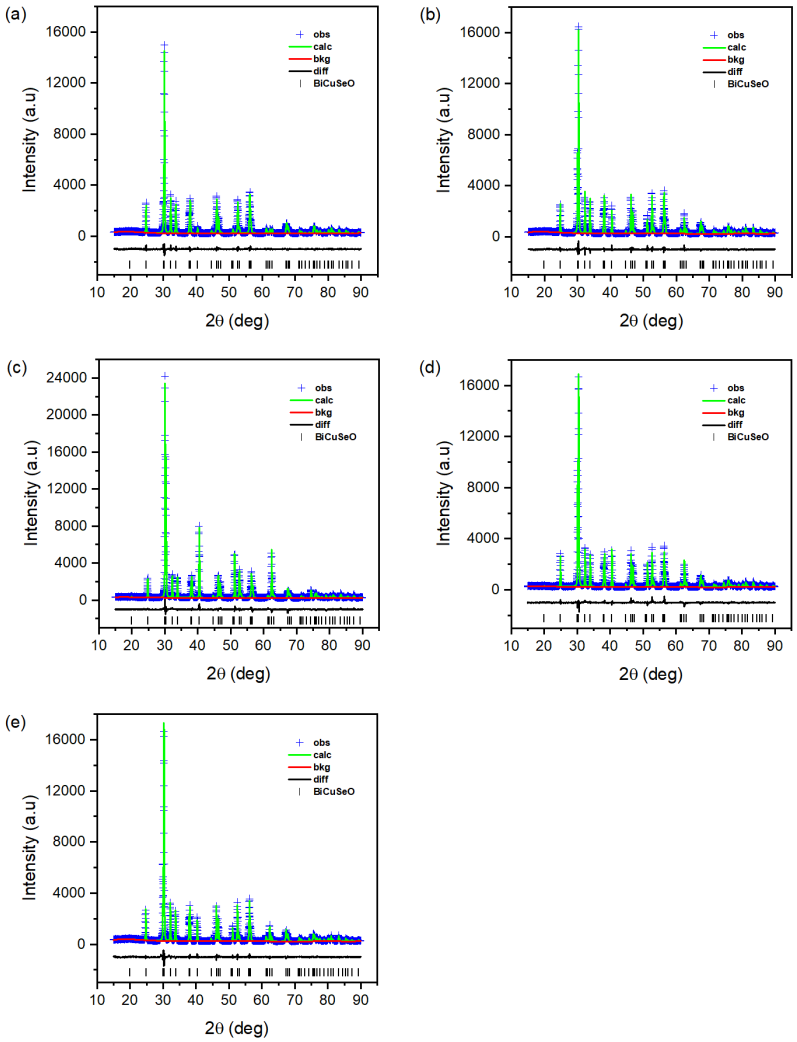

Figure S 1. Rietveld refinement plots of $BiCu_{1-x}Cr_xSeO$ (x = 0, 0.02, 0.04, 0.06 & 0.08) with observed intensity in blue symbol, calculated pattern in green, background in red, differences in black, and reference BiCuSeO as a solid line at the bottom of the figure

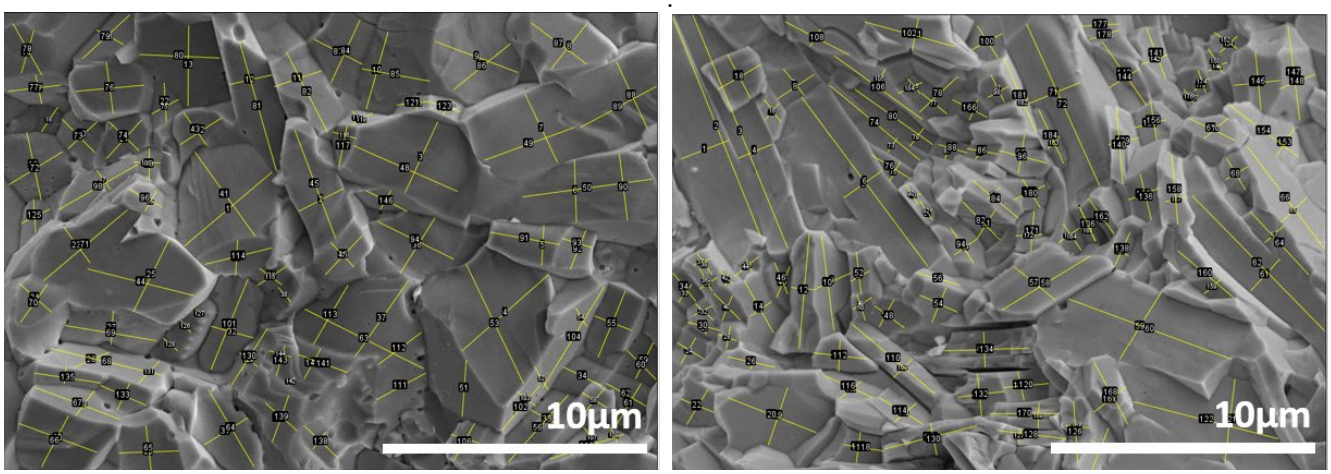

Figure S 2. Calculated grind size from SEM images

- The average grind size of pristine BiCuSeO and 4% Cr doped sample are 2.101 µm and 1.778 µm, respectively.
- The percentage of crystal size are 56% (below 2 µm), 35% (2-4 µm) and 9% (>4 µm) for Pristine BiCuSeO
- The percentage of crystal size are 69% (below 2 µm), 23% (2-4 µm) and 8% (>4 µm) for 4%Cr doped sample.

Reproducibility of the sample

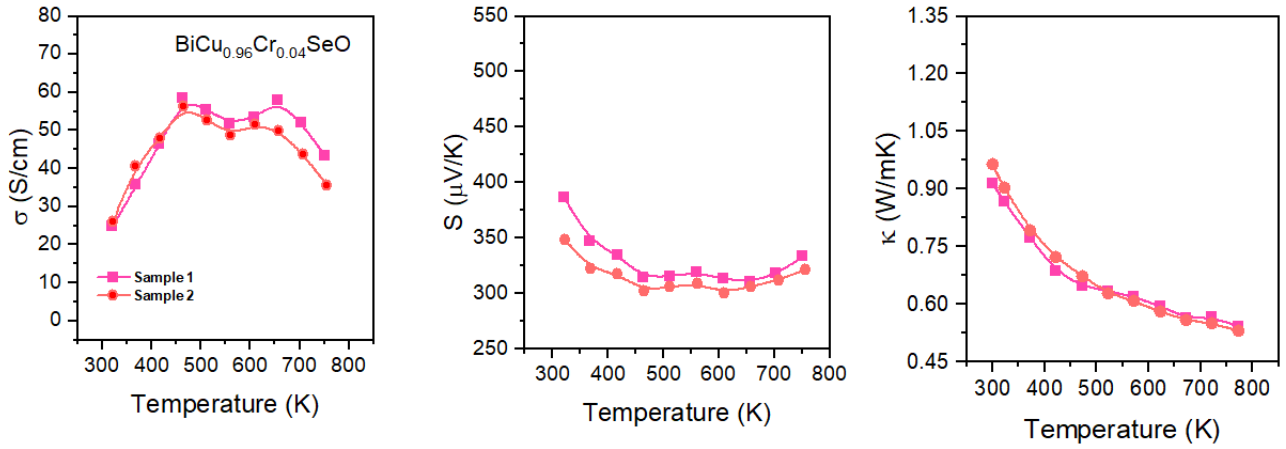

Figure S 3. The reproducibility of $BiCu_{0.96}Cr_{0.04}SeO$

These samples (sample 1 and 2) of the $BiCu_{0.96}Cr_{0.04}SeO$ were synthesized using the same method, and the results demonstrate good reproducibility among the samples.

Specific Heat Calculation & Thermal Diffusivity:

The temperature dependence of specific heat capacity is calculated using Debye model when $T > \theta_D$ with following equation

$$C_p = \gamma T + \frac{9Rn}{M} \cdot \left(\frac{T}{\theta_D}\right)^3 \cdot \int_0^{\theta_D/T} \frac{x^4 e^x}{(e^x-1)^2} dx \quad \text{(S1)}$$

where γ is the Sommerfeld coefficient, $\gamma = 3.075 \cdot 10^{-7}$ J g^{-1} K^{-2} [1], R is the ideal gas constant, n is the number of atoms, M is the molar mass, θ_D is the Debye temperature, $\theta_D = 243$ K [2], and $x = h\nu/k_B T$. The Debye temperature and the Sommerfeld coefficient were assumed to be independent of the doping level. According to equation (S1), the calculated specific heat capacity of the $BiCu_{1-x}Cr_xSeO$ samples is slightly higher than pristine BiCuSeO due to the atomic mass difference between Cr (51.9961) and Cu (63.546) atoms. The thermal diffusivity is measured by laser flash method using LFA427, Netzsch, Germany. The typical dimension that used in thermal diffusivity measurement is 10 mm in diameter with a thickness of approximately ~1.7 mm.

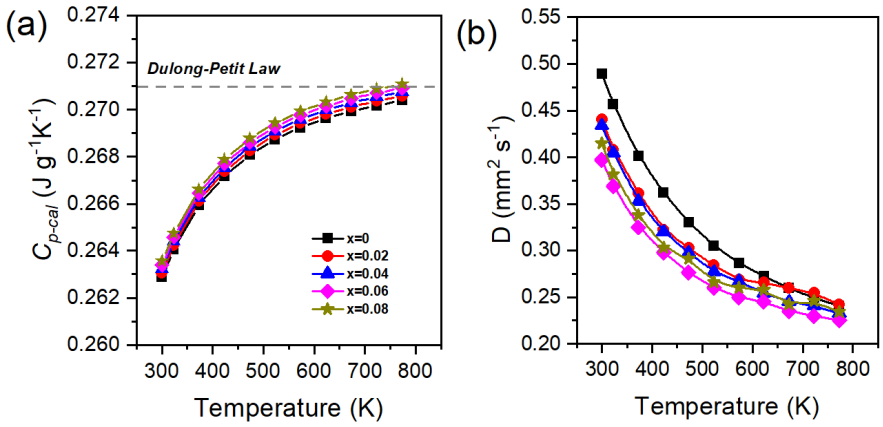

Figure S 4. Thermal properties as a function of temperature of the $BiCu_{1-x}Cr_xSeO$ (x = 0; 0.02; 0.04; 0.06; 0.08) (a). Specific heat capacity, (b). Thermal diffusivity.

Reference:

[1]. C. Barreteau, D. Bérardan, E. Amzallag, L.D. Zhao, N. Dragoe, Structural and electronic transport properties in Sr-doped BiCuSeO, Chemistry of Materials 24 (2012) 3168–3178. https://doi.org/10.1021/cm301492z

[2]. L. Pan, D. Bérardan, L. Zhao, C. Barreteau, N. Dragoe, Influence of Pb doping on the electrical transport properties of BiCuSeO, Appl Phys Lett 102 (2013). https://doi.org/10.1063/1.4775593/975500.

Lorenz number calculation & electronic thermal conductivity:

The total thermal conductivity (κ_{tot}) is defined as a sum of the electronic (κ_{ele}) and lattice thermal conductivity (κ_{lat}). The electronic part κ_{ele} is directly proportional to the electrical conductivity σ through the Wiedemann-Franz relation, $\kappa_e = L\sigma T$, where L is the Lorenz number [3]. The Lorenz number depends on the scattering parameter r and will decrease as the reduced Fermi energy η decreases with increasing temperature. The Lorenz number can be given as: [4]

$$L = \left(\frac{k_B}{e}\right)^2 \left(\frac{(r+\frac{7}{2})F_{r+\frac{5}{2}}(\eta)}{(r+\frac{3}{2})F_{r+\frac{1}{2}}(\eta)} - \left[\frac{(r+\frac{5}{2})F_{r+\frac{3}{2}}(\eta)}{(r+\frac{3}{2})F_{r+\frac{1}{2}}(\eta)}\right]^2 \right) \quad \text{(S2)}$$

For the Lorenz number calculation, we should get reduced Fermi energy η firstly; the calculation of η can be derived from the measured Seebeck coefficients by using the following relationship:

$$S = \pm\frac{k_B}{e}\left(\frac{(r+\frac{5}{2})F_{r+\frac{3}{2}}(\eta)}{(r+\frac{3}{2})F_{r+\frac{1}{2}}(\eta)} - \eta\right) \quad \text{(S3)}$$

where $F_n(\eta)$ is the $n-$th order Fermi integral,

$$F_n(\eta) = \int_0^\infty \frac{\chi^n}{1+e^{\chi-\eta}}\, d\chi \quad \text{(S4)}$$

$$\eta = \frac{E_f}{k_B T} \quad \text{(S5)}$$

where, k_B, e, and E_f are the Boltzmann constant, the electron charge, and the Fermi energy. By assuming that the acoustic phonon scattering ($r = -1/2$) is the main scattering mechanism, the Lorenz number can be obtained by applying the calculated reduced Fermi energy η and scattering parameter r into Eq. (S2). Table S1 shows the calculated Lorenz number based on SPB and APS model at room temperature. Figures S4 (a-b) show the Lorenz number and electronic thermal conductivity of the $BiCu_{1-x}Cr_xSeO$ as a function of temperature.

Table S1. The Lorenz number estimated by single parabolic band (SPB) and acoustic phonon scattering (APS)

T	S_{exp}	$S_{(SPB-APS)}$	η	F_0	F_1	F_2	L
K	(μVK^{-1})	(μVK^{-1})					($W\Omega K^{-2}$) × 10^{-8}
306	497.9700	497.970046	-3.759310	0.02303261	0.023166	0.04646502	1.49349976
322	491.7153	491.715306	-3.685950	0.02476414	0.024918	0.04999062	1.49382208
369	488.6485	488.648496	-3.649959	0.02566011	0.025825	0.05181673	1.49398886
417	488.1436	488.143586	-3.644032	0.0258107	0.025978	0.05212376	1.49401689
464	484.5475	484.547548	-3.601806	0.02690907	0.027091	0.0543643	1.49422135
512	467.7214	467.721412	-3.403896	0.03270285	0.032971	0.06621334	1.49529983
561	446.4189	446.419684	-3.152419	0.04186006	0.0423	0.08504593	1.49700436
610	428.9862	428.986208	-2.945652	0.05123263	0.051893	0.10445513	1.49874892
659	418.8106	418.810662	-2.824485	0.05764527	0.058481	0.11781312	1.49994249
707	411.2923	411.292365	-2.734698	0.06289362	0.063889	0.12879337	1.50091933
756	404.3442	404.344212	-2.651502	0.06816796	0.069338	0.13987131	1.50190099

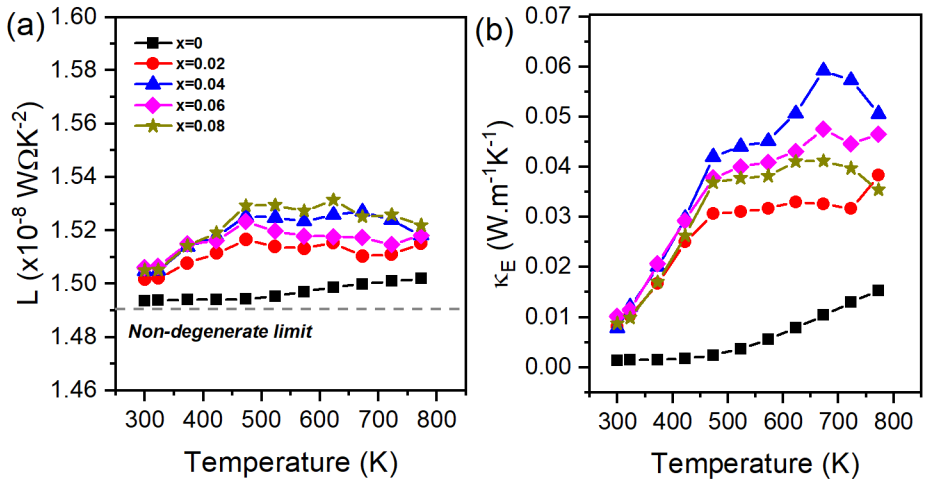

Figure S 5. (a) Lorenz number, (b) electronic thermal conductivity of the $BiCu_{1-x}Cr_xSeO$ (x = 0; 0.02; 0.04; 0.06; 0.08) as a function of temperature.

[3] Fitsul, V. I. *Heavily Doped Semiconductors*; Plenum Press: New York, 1969.

[4] Zhao, L.-D.; Lo, S.-H.; He, J. Q.; Li, H.; Biswas, K.; Androulakis, J.; Wu, C.-I.; Hogan, T. P.; Chung, D.-Y.; Dravid, V. P.; Kanatzidis, M. G. *J. Am. Chem. Soc.* **2011**, *133*, 20476.

Callaway model calculation:

In a solid solution system, point defects scattering originates from both the mass difference (mass fluctuations) and the size and the interatomic coupling force differences (strain field fluctuations) between the impurity atom and the host lattice. Callaway model has been applied to describe the influence of point defects on the lattice thermal conductivity [5−7]. We present a phonon scattering model based on the above theory and try to describe the effect of Cr doping on the lattice thermal conductivity of BiCuSeO system.

At temperature above the Debye temperature, the ratio of the lattice thermal conductivities of a material containing defects to that of the parent material can be written as: [5−7]

$$\frac{\kappa_{lat}}{\kappa_{lat,p}} = \frac{tan^{-1}(u)}{u} \tag{S6}$$

where κ_{lat}, $\kappa_{lat,p}$ are the lattice thermal conductivities of the defected and parent materials, respectively, and the parameter u is defined by:

$$u = \left(\frac{\pi^2 \theta_D \Omega}{h v_a^2} \kappa_{L,p} \Gamma\right)^{\frac{1}{2}} \tag{S7}$$

where h, Ω, v_a and θ_D stand for the Planck constant, average volume per atom, lattice sound velocity, and the Debye temperature.

$$v_a = \left(\frac{1}{3}\left[\frac{1}{v_l^3} + \frac{2}{v_s^3}\right]\right)^{-\frac{1}{3}} \tag{S8}$$

Here, the longitudinal (v_l, 3290m/s) and transverse (v_s,1900m/s) sound velocities have been obtained from previous research which gives v_a about 2107 m/s. Debye temperature θ_D is defined by: [8]

$$\theta_D = \frac{h}{k_B}\left[\frac{3N}{4\pi V}\right]^{\frac{1}{3}} v_a \tag{S9}$$

where the V is the unit−cell volume, N is the number of atoms in a unit cell, k_B is Boltzmann parameter, and h presents the Planck constant. Eq. (S9) gives θ_D about 243 K.

The disorder scattering parameter Γ in Eq. (S7) represents the strength of point defects phonon scattering, which includes two components, the scattering parameter due to mass fluctuations Γ_M and the scattering parameter due to strain field fluctuations Γ_S. A phenomenological adjustable parameter ε is always included because of uncertainty of Γ_S, one writes $\Gamma = \Gamma_M + \varepsilon\Gamma_S$. In this paper, ε is directly estimated by following relationship: [9]

$$\varepsilon = \frac{2}{9}\left(\frac{(7+6.4)\times\gamma(1+\upsilon_p)}{(1-\upsilon_p)}\right)^2 \tag{S10}$$

where υ_p the Poisson ratio, which can be derived from the longitudinal (v_l) and transverse (v_s) sound velocities by the relationship as: [5-7, 9]

$$\upsilon_p = \frac{1-2\left(\frac{v_s}{v_l}\right)^2}{2-2\left(\frac{v_s}{v_l}\right)^2} \tag{S11}$$

Eq. (6) gives υ_p about 0.25.

Gruneisen parameter (γ) has been calculated using Poisson ratio (υ_p) as: [5-7, 9]

$$\gamma = \frac{3}{2}\left(\frac{1+\upsilon_p}{2-3\upsilon_p}\right) \tag{S12}$$

Gruneisen parameter (γ) was calculated to be ~1.5 for BiCuSeO. Combination of Eq. (S10), (S11) and (S12), gives phenomenological adjustable parameter ε about 170.

There is no change on the sites of Bi, Se and O when the substitution between Cu and Cr occurs, $\Gamma_{Bi} = \Gamma_{Se} = \Gamma_O = 0$, which gives:

$$\Gamma_{BiCu_{1-x}Cr_xSeO} = \frac{1}{4}\left(\frac{M_{(Cu,Cr)}}{\bar{M}}\right)^2 \Gamma_{(Cu,Cr)} \tag{S13}$$

$$\Gamma = \Gamma_M + \Gamma_S \tag{S14}$$

$$\Gamma_{(Cu,Cr)} = \Gamma_{M,(Cu,Cr)} + \Gamma_{S,(Cu,Cr)} \tag{S15}$$

$$\Gamma_{M,(Cu,Cr)} = x(1-x)\left(\frac{\Delta M}{M_{(Cu,Cr)}}\right)^2 \tag{S16}$$

where $\Delta M = M_{Cu} - M_{Cr}$, and $M_{(Cu,Cr)} = (1-x)M_{Cu} + xM_{Cr}$

$$\Gamma_{S,(Cu,Cr)} = x(1-x)\left(\frac{\Delta r}{r_{(Cu,Cr)}}\right)^2 \tag{S17}$$

,

where $\Delta r = r_{Cu} - r_{Cr}$, and $r_{(Cu,Cr)} = (1-x)r_{Cu} + xr_{Cr}$

then,

$$\Gamma_{(Cu,Cr)} = x(1-x)\left[\left(\frac{\Delta M}{M_{(Cu,Cr)}}\right)^2 + \varepsilon\left(\frac{\Delta r}{r_{(Cu,Cr)}}\right)^2\right] \tag{S18}$$

and then,

$$\Gamma_{BiCu_{1-x}Cr_xSeO} = \frac{1}{4}\left(\frac{M_{(Cu,Cr)}}{\bar{M}}\right)^2 x(1-x)\left[\left(\frac{\Delta M}{M_{(Cu,Cr)}}\right)^2 + \varepsilon\left(\frac{\Delta r}{r_{(Cu,Cr)}}\right)^2\right] \tag{S19}$$

After the calculation of point defects scattering on phonon for Γ from those relative physical properties, we obtained perfect agreement between the calculated and measured values.

Table S2. The disorder parameters, measured κ_L, calculated κ_L and the difference between measured and calculated κ_L

x	Γ	κ_L (exp) ($Wm^{-1}K^{-1}$)	κ_L (calc) ($Wm^{-1}K^{-1}$)	diff (%)
0	0	1.09293	1.092884	0.004198
0.02	6.71678E-04	0.96804	1.015331	4.885215
0.04	1.29746E-03	0.95454	0.958083	0.371167
0.06	1.87889E-03	0.88892	0.91386	2.805652
0.08	2.41747E-03	0.9091	0.878624	3.352301

The theoretical calculation of lattice thermal conductivity is performed according to the Callaway model [10].

$$\kappa_L = \frac{k_B}{2\pi^2 v_s}\left(\frac{k_B T}{\hbar}\right)^3 \int_0^{\theta_D} \tau_{tot}\frac{x^4 e^x}{e^x - 1}dx \tag{S20}$$

where x is the reduced frequency ($x = \hbar\omega/k_B T$), ω the phonon angular frequency, k_B the Boltzmann constant, v_s the average sound speed, $\hbar$ the reduced Planck constant, θ_D the Debye temperature, and τ_{tot} the combined phonon relaxation time. Assuming scattering channels are independent of each other, the τ_{tot} can be evaluated by Matthiessen's rule:

$$\tau_{tot} = \tau_U + \tau_{PD} + \tau_{GB} + \tau_{PE} \tag{S21}$$

where τ_U, τ_{PD}, τ_{GB}, τ_{PE} are the relaxation time for Umklapp process (U), point defect scattering (PD), phonon – electron scattering (PE), and grain boundary scattering (GB), respectively.

The relaxation time for point defect scattering is showed as follows: [11]

$$\frac{1}{\tau_{PD}} = A\omega^4; A = \frac{V_a}{4\pi v_s^3}\Gamma \tag{S22}$$

where A is the fitting parameter, ω the phonon angular frequency, v_S is the average sound speed, V_a the atomic volume of the compound, Γ the disorder scattering parameter that characterizes the phonon scattering cross section of point defects. If we only consider Cr doping on Cu-site in BiCuSeO, Γ can be calculated by following equation S13 – S19 [12,13].

The relaxation time for Umklapp scattering at high temperature is [11]:

$$\frac{1}{\tau_U} = B\omega^2 T \tag{S23}$$

where B is a constant, ω the phonon angular frequency,and θ_D the Debye temperature.

The relaxation time for the grain boundary scattering is:

$$\frac{1}{\tau_{GB}} = \frac{v_S}{d} \tag{S24}$$

where v_s the average sound speed and d is the average grain size.

The relaxation time for the phonon – electron scattering is:

$$\frac{1}{\tau_{PE}} = C\omega T \tag{S25}$$

where C is a fitting parameter and ω the phonon angular frequency.

Since the value of B depends solely on the crystal structure of BiCuSeO, we determined its precise value by fitting Eq. S20-25 to the lattice thermal conductivity of pure BiCuSeO. Table S3 presents the obtained value of B alongside the calculated value of A. Consequently, the only adjustable parameter, C, for various levels of Cr-doping can be derived by fitting Eq. S20-35 to the measured lattice thermal conductivity data.

Table S3. Fitting parameters of calculated lattice thermal conductivity κ_L using Callaway model.

x	A (10^{-42} s^3)	B (10^{-17} sK^{-1})	C (10^{-4})
0	0.0012	3.0955	0.0001
0.02	2.3206	3.0955	37.41
0.04	4.4819	3.0955	19.23
0.06	6.4892	3.0955	17.56
0.08	8.3478	3.0955	0.33

[5] Callaway, J.; Von Baeyer, H. C. *Phys. Rev.* **1960**, *120*, 1149;

[6] Dey, T. K.; Chaudhuri, K. D. *J. Low. Temp. Phys.* **1976**, *23*, 419;

[7] Yang, J.; Meisner, G. P.; Chen, L. *Appl. Phys. Lett.* **2004**, *85*, 1140.

[8] K. Kurosaki, A. Kosuga, H. Muta, M. Uno, S. Yamanaka, *Appl. Phys. Lett*. **2005**, *87*, 061919.

[9] C. L. Wan, W. Pan, Q. Xu, Y. X. Qin, J. D. Wang, Z. X. Qu, M. H. Fang, *Phys. Rev. B* **2006**, *74*, 144109.

[10]. Callaway, J.; *Phys. Rev.* **1959**, *113*, 1046–1051.

[11]. P. G. Klemens, *Proc. Phys. Soc. Lond. A.*, **1955**, *68*, 1113-1128.

[12]. B. Abeles, *Phys. Rev.*, **1963**, 131, 1906.

[13]. G. A. Slack, *Phys. Rev.*, **1962**, 126, 427